We are IntechOpen,
the world's leading publisher of
Open Access books
Built by scientists, for scientists

6,900
Open access books available

185,000
International authors and editors

200M
Downloads

Our authors are among the

154
Countries delivered to

TOP 1%
most cited scientists

12.2%
Contributors from top 500 universities

CLARIVATE ANALYTICS

BOOK CITATION INDEX

INDEXED

WEB OF SCIENCE™

Selection of our books indexed in the Book Citation Index
in Web of Science™ Core Collection (BKCI)

Interested in publishing with us?
Contact book.department@intechopen.com

Laser Pulse Patterning on Phase Change Thin Films

Jingsong Wei[1] and Mufei Xiao[2]
[1]Shanghai Institute of Optics and Fine Mechanics,
Chinese Academy of Sciences
[2]Centro de Nanociencias y Nanotecnología,
Universidad Nacional Autónoma de México
[1]China
[2]México

1. Introduction

In the present chapter, we discuss the formation of microscopic patterns on phase change thin films with low power laser pulses. The discussions are mostly based on our recent experimental and theoretical results on the subject.

Phase change thin films are widely used as optical and electric data storage media. The recording is based on the phase change between the crystalline and amorphous states. In the writing process, a small volume in the thin film is locally and rapidly heated to above the melting point and successively quenched into the amorphous phase. In the erasing process, the material undergoes a relatively long heating to reach a temperature above the glass transition but yet below the melting point, which brings the material back to the crystalline phase.

However, during the writing process, apart from the phase changes, physical deformation of the surface occurs, which often creates bumps of various forms. In other words, low intensity laser pulses are able to microscopically form patterns on phase change films. The formed patterns modify the topographic landscape of the surface and bring about variations on the material properties of the films. The modifications can be harmful or helpful depending on what kind of applications one looks for. Therefore, in order to properly deal with the laser induced bumps, it is essential to understand the process of bump formation, and to qualitatively and quantitatively describe the created bumps as well as its relation with the laser pulse parameters, such as the beam distributions and the average intensity etc. so that one is able to closely control the formation of microscopic patterns on phase change films with low power laser pulses. Recently, we have systematically studied the formation of bumps during laser writing both experimentally and theoretically.

In the present chapter we shall round up the important results from our studies and present detailed discussions on the results. We organize the chapter as follows. In the first part, we present results of forming circular bumps as a by-production of rather conventional laser writing process for the purpose of data storage on $Ag_8In_{14}Sb_{55}Te_{23}$ chalcogenide phase change films. In this part, the detailed process of writing and erasing will be described, and

the experimental and theoretical characterizations of the bumps are demonstrated. In the second part, we expand our work to intentionally form micro patterns on multilayer ZnS–SiO$_2$/AgO$_x$/ZnS–SiO$_2$ thin films by laser direct writing technology. We shall conclude the work in the end of the chapter.

2. Laser pulse induced bumps in chalcogenide phase change films

Chalcogenide phase change thin films are widely used as optical and electric data storage media. The recording is based on the phase change between the crystalline and amorphous states (Kolobov et al., 2004; Kalb et al., 2004; Welnic et al., 2006; Wuttig & Steimer, 2007). In the writing process, a small volume in the thin film is locally and rapidly heated to above the melting point and successively quenched into the amorphous phase. In the erasing process, the material undergoes a relatively long heating to reach a temperature above the glass transition but yet below the melting point, which brings the material back to the crystalline phase. The heat source for the phase change is usually from laser pulses in optical data storage, or electric current pulses in electric data storage. In the present work we shall selectively concentrate on the optical storage.

In the process of amorphization, i.e., the laser writing process, the material experiences a volume change due to the stronger thermal expansion in the melting state than in the crystalline state, as well as the density difference between the two states. Therefore, the amorphous recording marks are actually physically deformed as circular bumps because the amorphous recording marks inherit the volume in the melting state after a fast cooling stage. Subsequently, the bumps may cause further deformation in other thin layers stacked underneath as in the cases of optical information memory in optical storage and the electrode in electric storage. While slight deformation in the writing process is inevitable, significant bumps are harmful for the storage media as they affect dramatically the size of the marks, which eventually reduces the recording density of the media, and shorten the durability of the device. In extreme cases the bumps may grow so big that a hole is formed at the apex of the bump. Therefore, to quantitatively describe the bump formation is of great interest for storage applications.

We have established a theoretical model for the formation process, where the geometric characters of the formed bumps can be analytically and quantitatively evaluated from various parameters involved in the formation. Simulations based on the analytic solution are carried out taking Ag$_8$In$_{14}$Sb$_{55}$Te$_{23}$ as an example (Wei et al., 2008; Dun et al., 2010). The results are verified with experimental observations of the bumps.

2.1 Theory

Let us start by describing the amorphization process schematically in the volume-temperature diagram as shown in Fig. 1, where the principal paths for the phase changes are depicted. Initially, the chalcogenide thin film is considered in the crystalline state represented by point a; a laser or current pulse of nanosecond duration heats the material up to the melting state, which is represented by point b. Subsequently, the material is cooled quickly with a high rate exceeding $10^7 \, C/s$ to the room temperature to form the final amorphous mark. During the quenching stage, the material structure does not have sufficient time to rearrange itself and remains in the equilibrium state, and thus inherits the structure and volume at the melting state. Therefore, the volume has an increase ΔV, and

the mark appears as a bump. If the laser or current pulse injects energy higher than the ablated threshold corresponding to the vaporization temperature, the heating temperature reaches point *d*, and the material is then rapidly cooled to the room temperature, which is represented by point *e*; an ablated hole can be formed at the top of the bump.
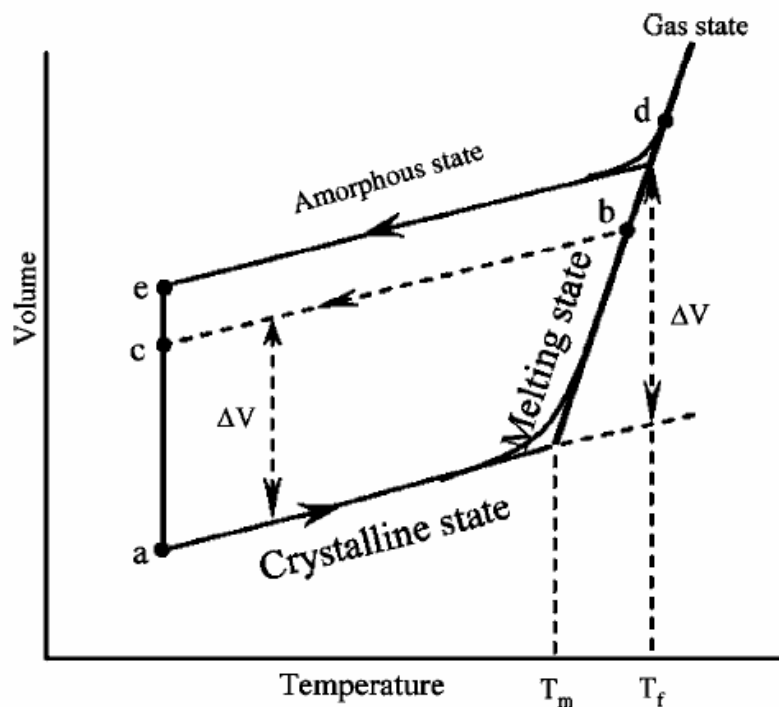

Fig. 1. Volume-temperature diagram of chalcogenide films. The film is heated by laser from point *a* to point *b* and returns to point *d*, or to point *c* and returns to point *e* after faster cooling.

The geometric characters of the bump are graphed in Fig. 2, where cross-sections of the circular bump are schematically shown respectively for the case of a bump and the case of a bump with a hole on its top. It is worth noting that, in general, the volume thermal expansion coefficient for chalcogenide thin films has two different constant values in the crystalline and melting states, respectively. In our analysis, there is assumed a Gaussian intensity profile for the incident laser pulse, and volume changes occur only in the region irradiated by the laser pulse, as shown in Fig. 2(a). If the laser pulse energy exceeds the ablated threshold, a hole is to be formed at the top of the bump, which is shown in Fig. 2(b). Mathematically, for the fast heating and amorphization process, the net volume increase can be written as $\Delta h = (\beta_m - \beta_c) \cdot V_0 \cdot (T_{surf} - T_m)$, where β_m and β_c are the volume thermal expansion coefficients in the crystalline and melting states, respectively. V_0 is the irradiated region volume. T_{surf} is the material surface temperature heated by laser pulse and T_m is the temperature corresponding to the melting point. Since the irradiated region is axially symmetric due to the Gaussian laser beam intensity profile, the bump height can be expressed as

$$\Delta h(r) = (\beta_m - \beta_c) \cdot h_0(r) \cdot (T_{surf} - T_m) \tag{1}$$

where *r* is the radial coordinate, and $h_0(r)$ is the height of the irradiated region.
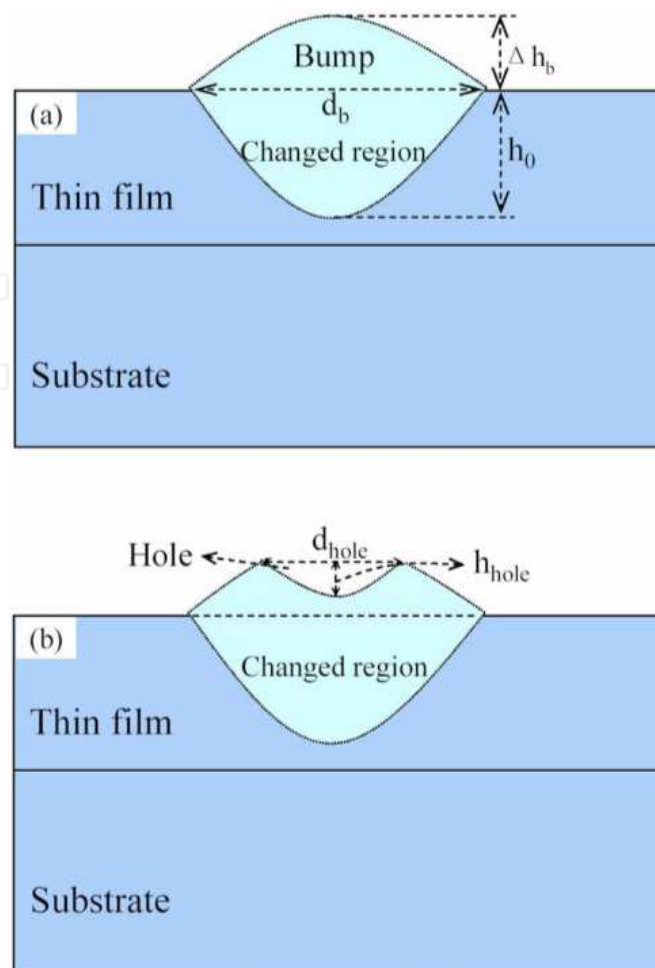
Fig. 2. Bump formation schematics: (a) bump and (b) hole on the top of bump.

Furthermore, the absorbed energy per unit volume and per unit time can be calculated by

$$g(r,z) = \alpha(1-R)\frac{2P}{\pi w^2}\exp(-\frac{2r^2}{w^2})\exp(-\alpha z) \tag{2}$$

where α is the absorption coefficient, R is the reflectivity of the material, P is the laser power, w is the laser beam radius at the $1/e^2$ of the peak intensity, and z is in the depth direction from the sample surface. In Eq. (2) the quantity $\alpha(1-R)$ is the absorbed part of the transmitted light, which decays exponentially $\exp(-\alpha z)$ along the z direction and spreads as a Gaussian function $\exp(-2r^2/w^2)$ in the r direction.

Generally for data storage, the width of the laser pulse is in the range from nanosecond to millisecond. Within this range, the temperature distribution in the irradiated region can be expressed as

$$T(r,z) = \frac{g(r,z)\tau}{\rho C_p} \tag{3}$$

where ρ is the density, C_p is the heat capacity of the material, and τ is the laser pulse width. According to (Shiu et al., 1999), the bump height $\Delta h(r)$ can be calculated, within the

temperature interval $T_m < T(r,0) < T_f$, where T_f is the temperature corresponding to the vaporization point above which the material will be ablated, by

$$\Delta h(r) = \frac{\beta_m - \beta_c}{\alpha}\left[T(r,0) - T_m\right]\ln\left[\frac{T(r,0)}{T_m}\right] \tag{4}$$

and the bump diameter d_p can be calculated by setting $T(r,0) = T_m$ and $r = d_p/2$ in Eq. (3) with

$$d_p = \sqrt{2}w\sqrt{\ln\left[F_0\frac{\alpha(1-R)}{\rho C_p}\right]\frac{1}{T_m}} \tag{5}$$

where $F_0 = 2P\tau/\pi w^2$. Similar to the derivation of bump diameter, if the laser pulse energy exceeds the ablated threshold, an ablated hole is formed when $T(r,0) > T_f$ and the hole diameter in the bump d_{hole} can be calculated as

$$d_{hole} = \sqrt{2}w\sqrt{\ln\left[F_0\frac{\alpha(1-R)}{\rho C_p}\right]\frac{1}{T_f}} \tag{6}$$

It should be noted that in our analytical model, the thermo-physical parameters of material are assumed independent from temperature.

2.2 Experimental observations

Before presenting results of simulation based on the above developed formalism, let us show some experimental observations of the bumps. The experimental results provided useful and meaningful values for choosing the parameters involved in the theoretical simulations. In the experiments, $Ag_8In_{14}Sb_{55}Te_{23}$ thin films were directly deposited on a glass substrate by dc-magnetron sputtering of an $Ag_8In_{14}Sb_{55}Te_{23}$ target. The light source is a semiconductor laser of wavelength $\lambda = 650nm$, and the laser beam is modulated to yield a $50ns$ laser pulse. The laser beam is focused onto the $Ag_8In_{14}Sb_{55}Te_{23}$ thin film, and the light spot diameter is about $2\mu m$. In order to form bumps with different sizes, various laser power levels were adapted. Some of the experimental results are presented in Figs. 3–5.

Fig. 3(a) shows some bumps obtained with laser power $3.8mW$. The inset in Fig. 3(a) is an enlarged image of one bump. The bump diameter is about $0.9 - 1.0\mu m$. In order to further analyze the bump morphology, an atomic force microscope (AFM) was used to scale the bump. The results are shown in Fig. 3(b), where the top-left inset shows the same bumps as in Fig. 3(a), and the top-right inset is the cross-section profile of the bump. One notes that the bump height is about $60 - 70nm$, and the diameter is about $1\mu m$. With the increase of laser power, a round hole in the bump is formed, as shown in Fig. 4, where the laser powers are 3.85, 3.90, and 4.0 mW, respectively. The corresponding bumps are shown from left to right in Fig. 4.

The bumps in Fig. 5(a) were produced at laser power level 4.0 mW. In Fig. 5(a) the left-bottom inset is an enlarged bump image. It is found that holes are formed in the central region of the bumps. Fig. 5(b) presents the AFM analysis, where the top-right inset is the three-dimensional bump image. It can be seen that the bump diameter is about $1\mu m$, and the size of the hole is about $250 - 300nm$.
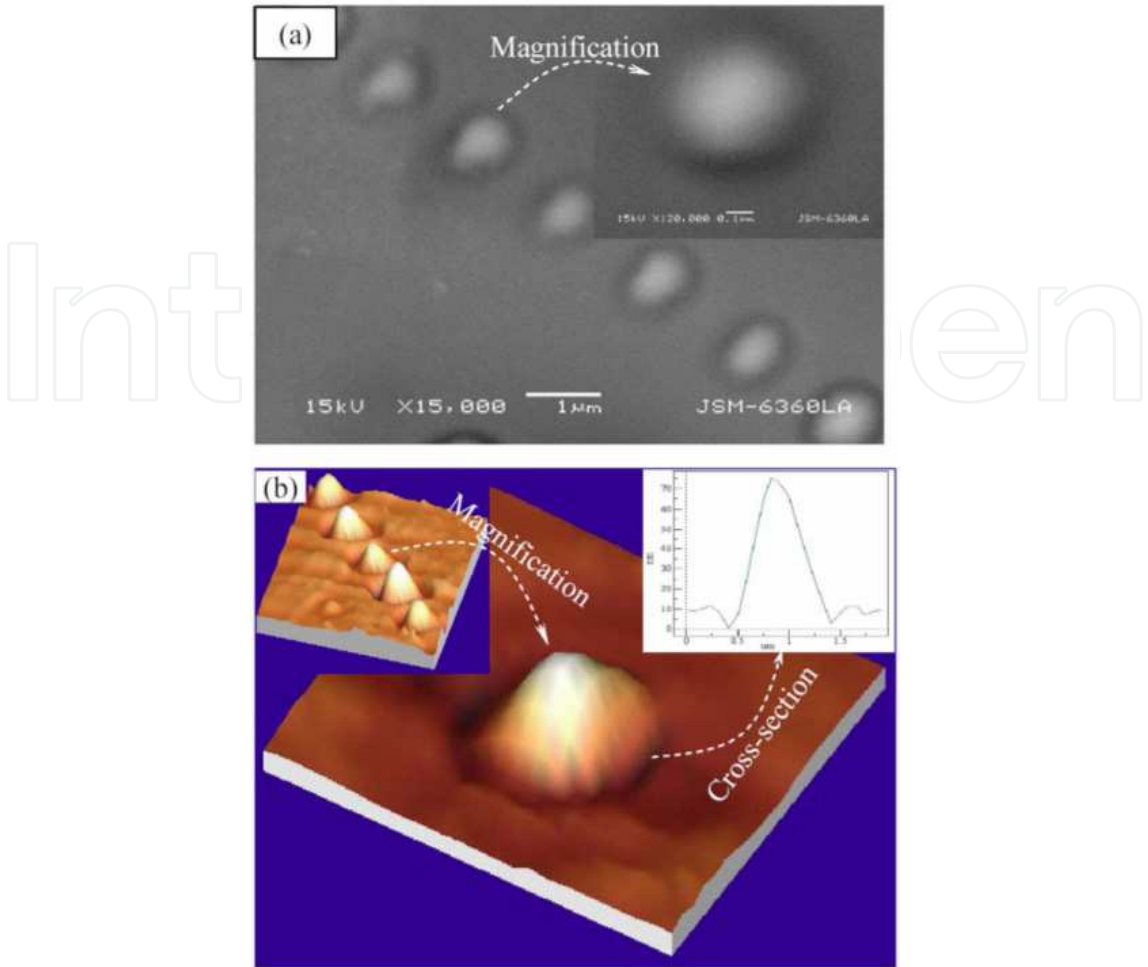
Fig. 3. Bumps formed at laser power $3.8mW$: (a) SEM analysis and (b) AFM analysis.
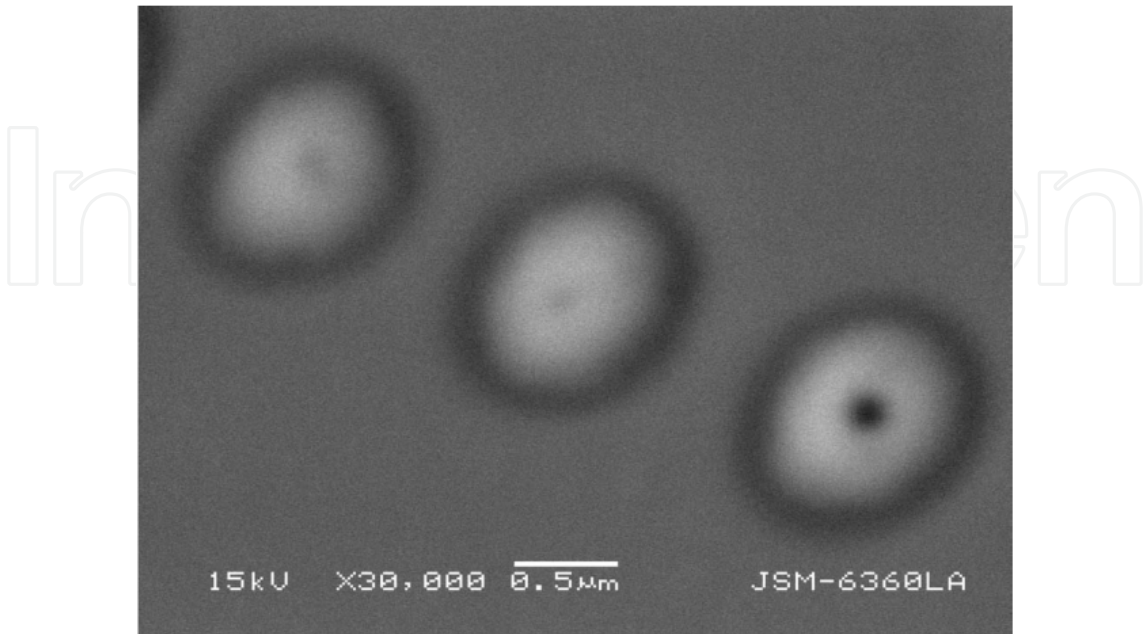

Fig. 4. SEM analysis for bumps formed at laser power of 3.85 , 3.90 and $4.0mW$.
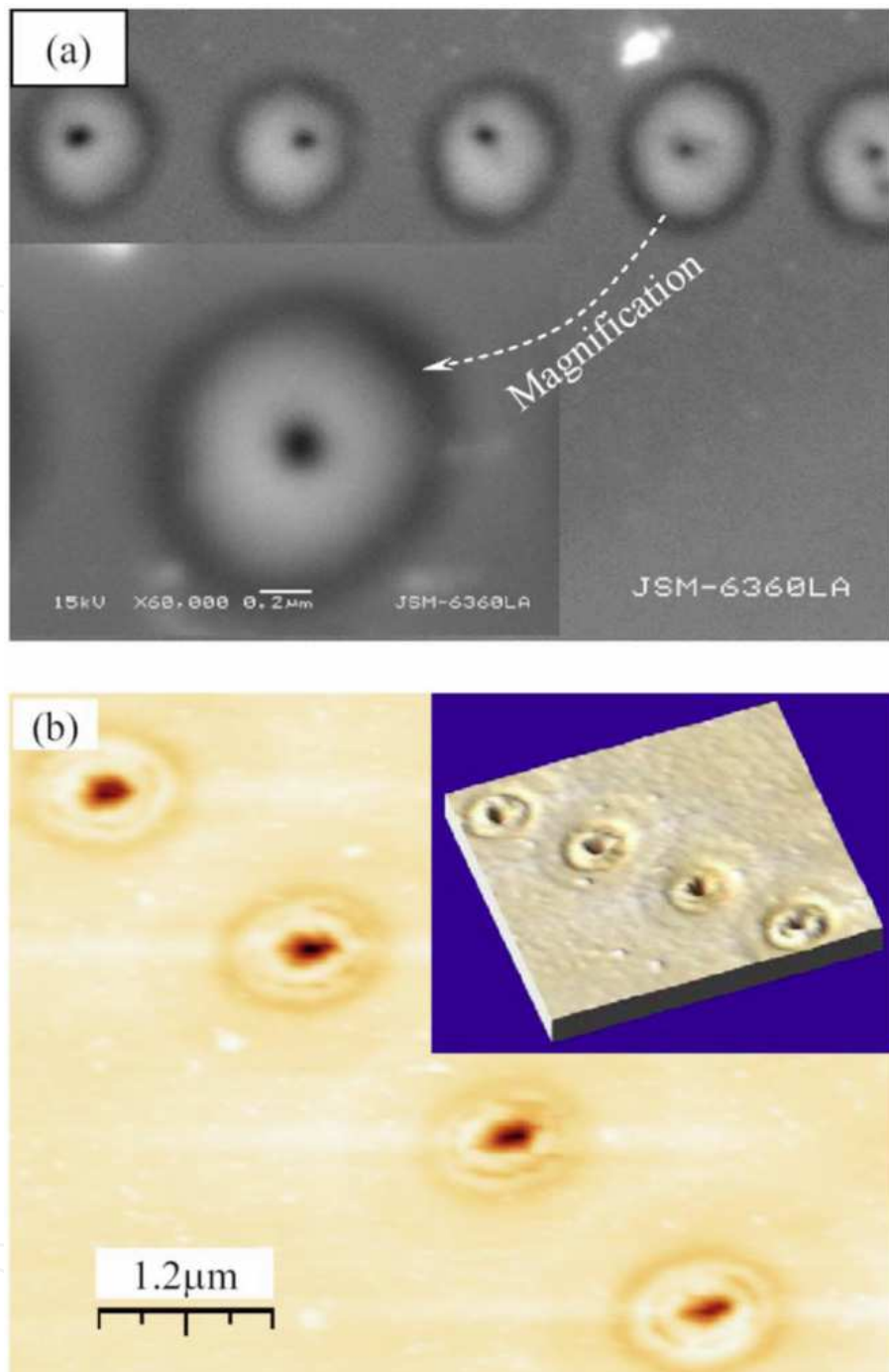
Fig. 5. Bumps formed at laser power 4.0 *mW*: (a) SEM analysis and (b) AFM analysis.

2.3 Numerical simulations

In this section, we present results of theoretical simulations based on the developed formalism. Calculations were carried out to simulate the experiments presented in the previous section, so that the numerical results can be compared with the experimental observations. Some parameters needed for the calculations were obtained from experiments. The melting and vaporization points of $Ag_8In_{14}Sb_{55}Te_{23}$ were measured by a differential scanning calorimeter (DSC), and the results are given in Fig. 6. It can be seen that the

melting T_m and vaporization T_f points are 512 °C and 738 °C, respectively. It should be noted that T_f is determined by the cross point between the tangent lines of AB and CD. The capacity C_P was also measured to be about $320J/KgK$ by the DSC method. The density is obtained by $\rho = \left(\rho_{Ag} \times 8 + \rho_m \times 14 + \rho_{Sb} \times 55 + \rho_{Te} \times 23\right)/100 = 6981.2 Kg/m^2$. The thermo-physical parameters used in the calculation are listed in Table I. The volume thermal expansion coefficients of Ag$_8$In$_{14}$Sb$_{55}$Te$_{23}$ thin film in the crystalline and melting states are difficult to measure, and we estimated that β_c and β_m were 25×10^{-6} / °C and 25×10^{-3} / °C, respectively. This is reasonable because the linear thermal expansion coefficient in liquid state is about ten times that in the solid state, therefore, the corresponding volume thermal expansion coefficient in the liquid state is about 10^3 times that in the solid state.
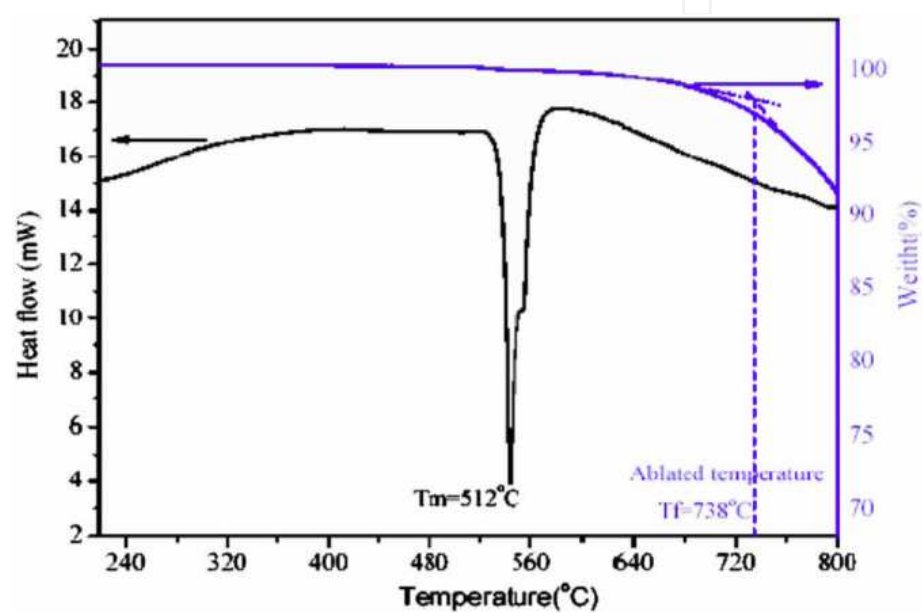

Fig. 6. DSC analysis for Ag$_8$In$_{14}$Sb$_{55}$Te$_{23}$ thin films.

With all the parameters assigned, simulations were carried out based on the developed formalism, and some of the simulation results in comparison with the above experimental observations are presented as follows. In Fig. 7, it shows the simulation results for laser power $P = 3.8mW$, which corresponds to the experimental situation in Fig. 3. Fig. 7(a) gives the temperature profile at different depth positions. One sees that the maximum temperature is about 720 °C at the centre of the thin film surface. At this temperature, a bump is to be formed, but the ablation is not to occur. This is shown in Fig. 7(b), where the bump height is about $70nm$. The bump diameter and area can be estimated from the top view of Fig. 7(b) to be about $847nm$ and $0.5636m^2$, respectively. These results are consistent with the experimental results in Fig. 3.

w (μm)	τ (ns)	α (m^{-1})	R	ρ (Kg m^{-3})	C_p (J Kg^{-1} K^{-1})	T_m (°C)	T_f (°C)	β_c (°C)	β_m (°C)
1.0	50	3×10^7	0.55	6981.2	320	512	738	25×10^{-3}	25×10^{-6}

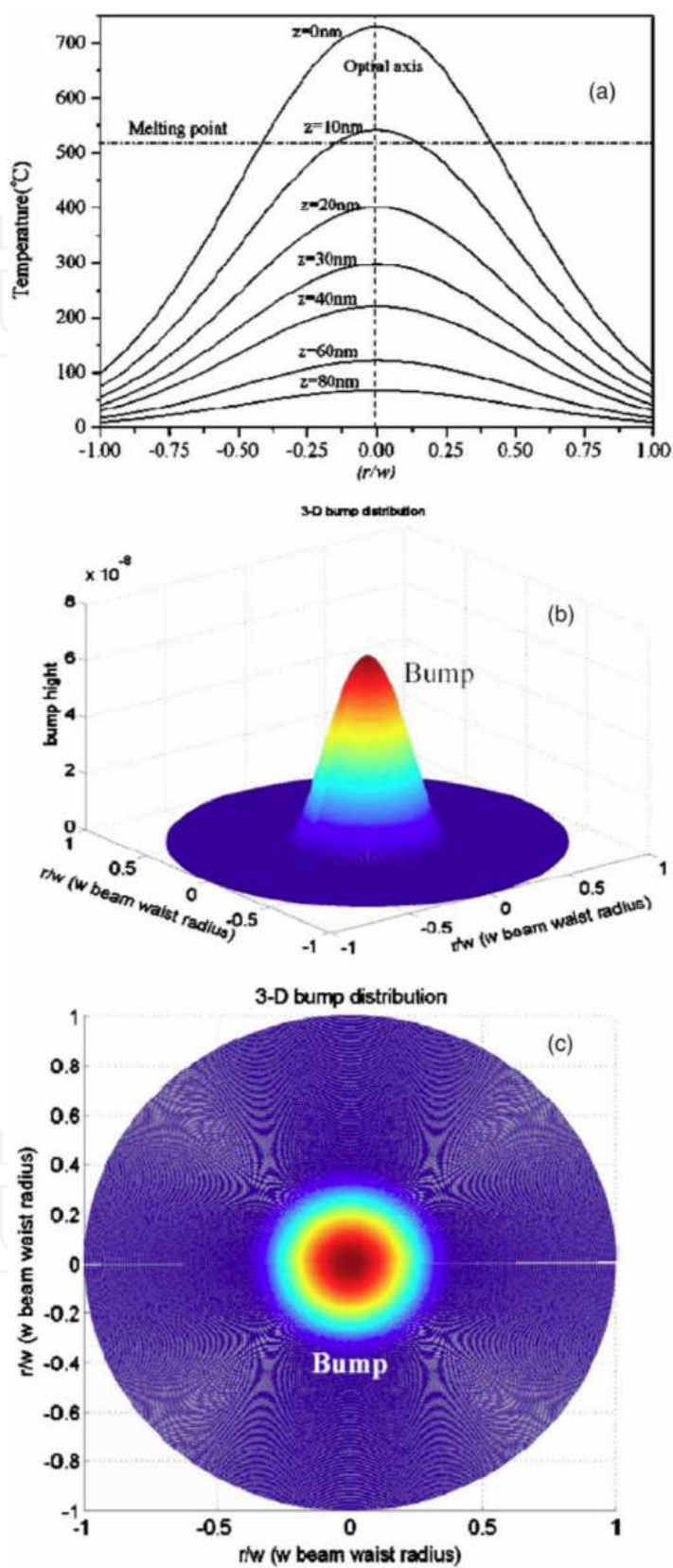Table 1. Thermo-physical and experimental parameters for the simulation.27

Fig. 7. Simulation results for laser power $3.8mW$: (a) temperature profile, (b) 3D image of bump, and (c) top-view of bump.
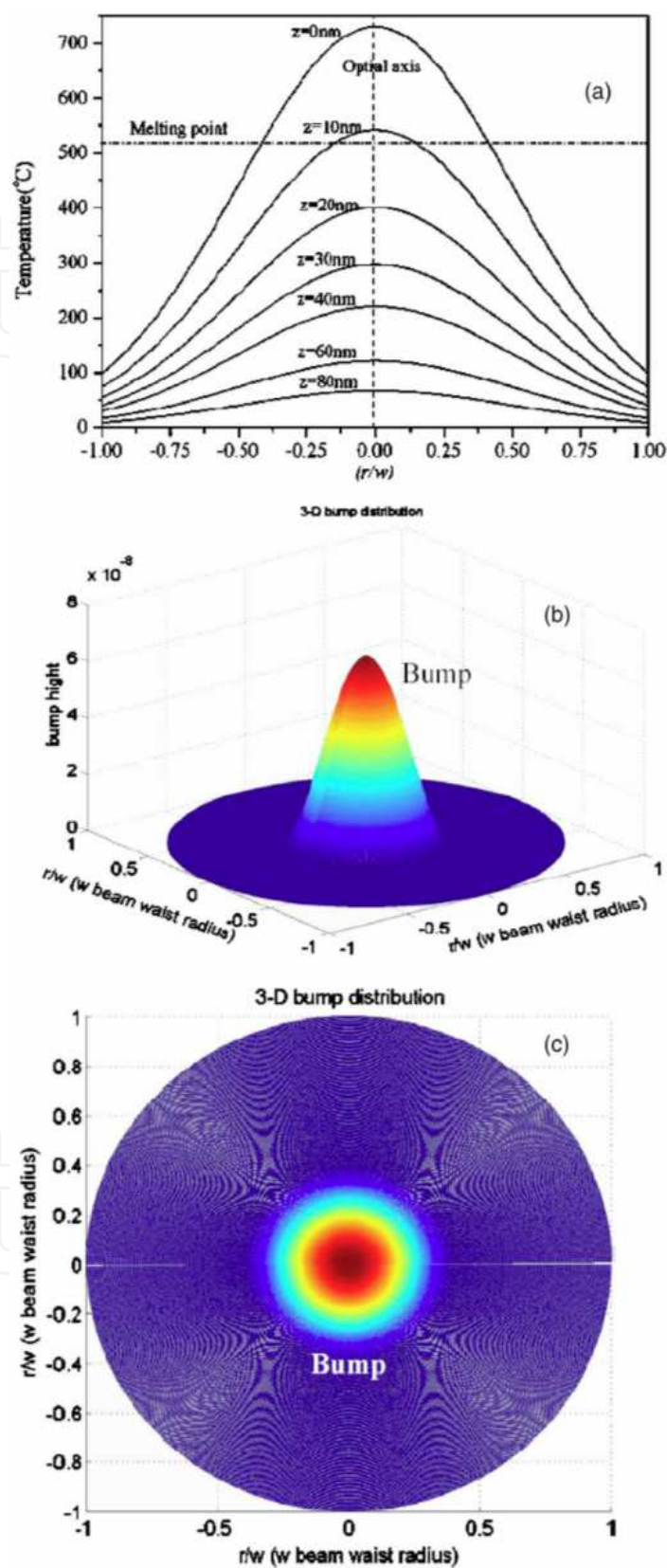
Fig. 8. Simulation results for laser power $4.0 mW$: (a) temperature profile and (b) hole formed at the top of bump.

With an increase of laser power, the temperature of thin films will exceed the vaporization point, and the ablation in the bump will take place. Fig. 8 shows the simulation results for laser power $P = 4.0mW$, which corresponds to the experimental situation in Fig. 5. In Fig. 8(a) the radial temperature is shown at different depth position. It can be seen that the maximum temperature at the centre of the sample surface reaches up to about $760\,°C$, which exceeds the vaporization point T_f ($738\,°C$), and indicates that the ablation may occur in the centre of the spot. The resulting ablation is shown in Fig. 8(b), where a two-dimensional ablation image is given. One realizes that the bump diameter and area are about $905nm$ and $0.644m^2$, respectively. It can also be seen that an ablation hole is formed in the centre of the bump, and the diameter of the hole is about $270nm$. One compares the simulation results in Fig. 8 to the experimental results in Fig. 5 and realizes that the model simulation is consistent with the experimental observation. This confirms the correctness and usefulness of the established model and the developed formalism.

3. Patterning on multilayer thin films with laser writing

Recently, pattern structures have been used widely in many fields, such as photonic crystal and solar cell industry, owing to its advantages over the common coatings. In the last several years, pattern structures have been fabricated on silicon, quartz, and especially photo-resist by many kinds of technologies, such as ultraviolet lithography (DUV), electron beam lithography, and focused ion-beam (FIB). However, most of the technologies are not suitable to fabricate large-area structures due to the time-consuming process and high-cost equipment. One of the most attractive and competitive technologies is laser direct writing technology, in which the structures are usually written on photo-resist. But photo-resist is often followed by developing and etching procedures after writing by laser beam, which definitely increases the time-consuming and cost and restricts the application of the structure.

AgOx material has been applied to photoluminescence (PL) emission field, nonlinear optics, and superconductive magnetic levitation due to its better performance. One of the most important applications is optical storage mask layer in super-resolution near-field structure (Super-RENS), and (Tominaga et al., 1999; Liu et al., 2001) have applied this structure to optical storage field using different recording layers, respectively. In this special structure, AgOx thin film layer is usually sandwiched by two protective layers (ZnS–SiO$_2$), i.e., (ZnS–SiO$_2$)/AgOx/(ZnS–SiO$_2$). In the present work, we used this structure to fabricate pattern by laser direct writing. Compared with photo-resist, the materials do not need developing and etching process, and the laser power is required to be in a very low range, so it is suitable to fabricate a large-area pattern structure in very short time and very low cost, which largely decrease the time-consuming and industrial cost.

3.1 Principle

It is well known that in an open system the AgO_x material is chemically known to decompose into Ag particles and O_2 at about 160°C. When the film structure is thermally heated beyond this temperature, AgOx layers will decompose to Ag and O_2 according to AgOx $\rightarrow$ Ag+x$_2$O$_2$. The decomposition reaction has been verified by many methods. When the laser beam irradiates on the AgOx film, a small volume of thin film is locally and rapidly

heated to above the decomposing temperature, and then the reaction happens. The oxygen released by the decomposition is stayed in the enclosed system, so it will apply pressure to surface. Generally speaking, the AgOx thin film with the thickness of about 10 nm was used in optical storage field as the mask film. While when the thickness is increased to more than 100 nm, it may produce a big oxygen bubble by the pressure and heat following the AgOx decomposition induced by the focused laser beam, and a huge volume expansion is formed at last, just as shown in Fig. 9(a). Fig. 9(b) shows the interior situation when AgOx decomposes into silver and oxygen. The O_2 and Ag particles are rough and tumble and filled the whole room. After the AgOx cooling down to the room temperature, the expanded volume will be left as bump. If we precisely control the laser parameters, the regular and uniform bump array pattern structure can be obtained.
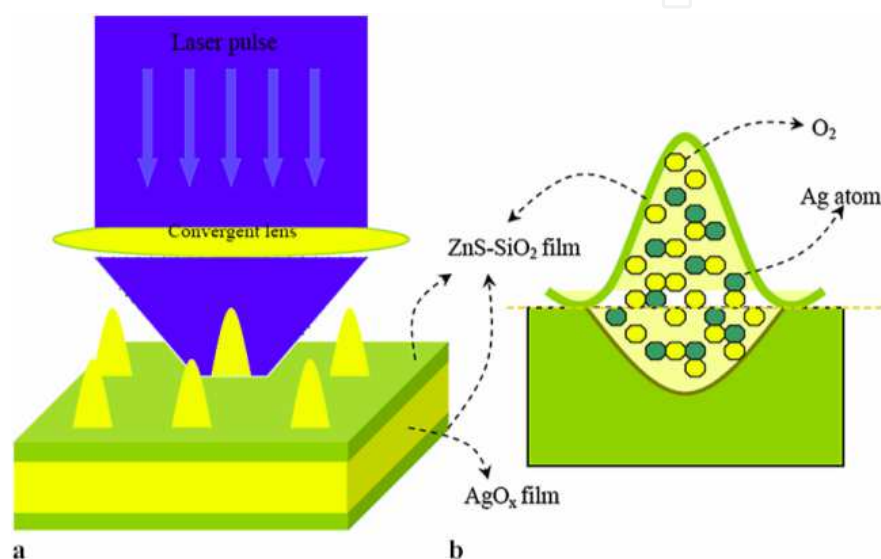
Fig. 9. Schematic of laser direct writing multilayered AgOx thin film. (a) Laser irradiated the thin film and the bubble formed. (b) Decomposition of AgOx and the formation of ZnS–SiO$_2$ bubble.

In fact, the layer structure is not a completely enclosed system; inter-diffusion between the as in the bump and the air outside occurs, which causes the pressure inside and outside the bump to reach up to balance. However, if the laser energy is very high and exceeds the ablation threshold of AgOx, the bumps may grow so big that a hole will form at the apex.

3.2 Experiments
According to the principle, the samples with a multilayer thin film structure "ZnS–SiO$_2$(10 nm)/AgOx(100 nm)/ZnS–SiO2(10 nm)" were prepared on glass substrates by radio frequency (RF) reactive magnetron sputtering. A pure Ag target with a diameter of 60 cm was bombarded by a gas mixture of Ar/O_2 plasma. In order to make more Ag particles react with O_2, we finally chose the ratios of $O_2/(O_2+Ar)$ at 0.9 and the sputtering power 50W. Then the AgOx film with a thickness of 100 nm was prepared, and the structural phase of the as-deposited AgOx film was identified by X-ray Diffraction (XRD). The ZnS–SiO$_2$ films were prepared by RF magnetron sputtering. The sputtering power was 100 W, and the thickness was 10 nm, correspondingly. After the samples were prepared, the laser direct writing was carried out with a laser wavelength of 488 nm. And the pattern structures were observed by atomic force microscope (AFM).
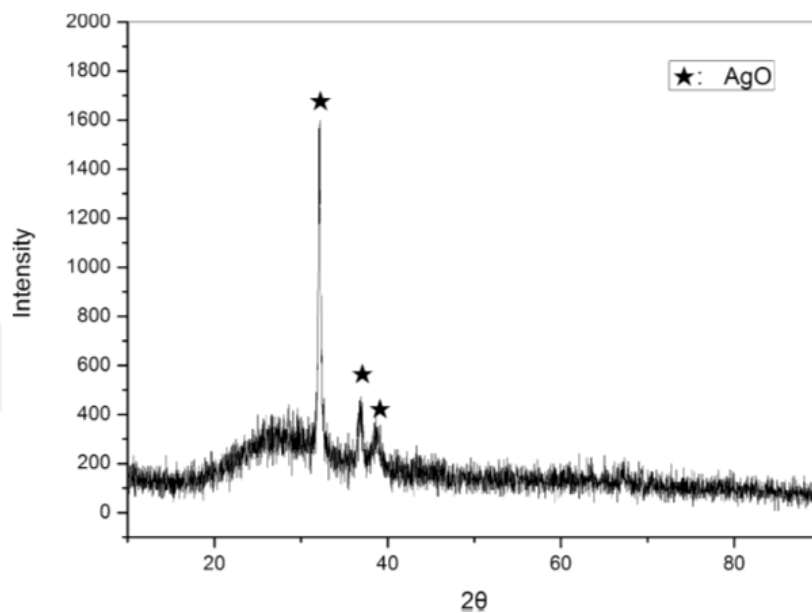
Fig. 10. XRD patterns of the as-deposited AgOx films prepared by RF reactive magnetron sputtering.

3.3 Results

Fig. 10 shows the XRD pattern of the as-deposited AgOx films. It was found that the main constituent is AgO, which agrees with the results of (Liu et al., 2001). Fig. 11 shows the pattern structures fabricated on multilayered "ZnS–SiO$_2$/AgOx/ZnS–SiO$_2$" sample, where the range of laser power is from 3.0 mW to 5.0 mW. From the Fig. 11 we can see that the pattern structure appears to be taper shape and very regular and uniform. The boundary between the area with and without laser irradiation is well defined as shown in Fig. 11(c), and the patterns are very steep with smooth wall. Fig. 11(a) and 11(c) show the three dimensional (3D) photos written by higher and lower laser powers, respectively.

Fig. 11(b) and 11(d) are the lateral photos of Figs. 11(a) and 11(c), respectively. One can find that the different pattern height can be realized by tuning the laser power. The larger the laser power, the higher the pattern. When the laser power is 5.0 mW, the height reaches the largest value. As the laser power decreases, the height gradually decreases to the lowest value at the laser power of 3.0 mW, where the pattern almost is undistinguishable. Fig. 12 shows the dependences of pattern structure height, diameter, and aspect ratio (aspect ratio = height/diameter) on laser power. We can find that both height and diameter increase with the laser power, as shown in Figs. 12(a) and 12(b). The range of the height is from 6 nm to 183 nm, and the diameter is from 482 nm to 912 nm, correspondingly. The aspect ratio is an important factor in pattern structure application. Generally speaking, the higher aspect ratio will possess a better performance. In this work, we find that the aspect ratios rapidly increase from the minimum of 0.012 at laser power of 3.0 mW to the maximum of 0.201 at laser power of 5.0 mW, which indicates that the better aspect ratio can be obtained in higher laser powers.

In order to obtain more details about the pattern structure, we amplify a small area from Fig. 11(a), and the result is shown in Fig. 13(a). It can be seen that the pattern structures appear taper shape and are very regular and uniform. The boundary between the area with and without laser irradiation is well defined, and the patterns are very uniform and smooth.

We also chose six pattern units (marked by line in Fig. 13(b)) to measure the height and diameter of the structures, and the result is shown in Fig. 13(c). One notes that the height of pattern is about 150 nm, and the diameter is around 650 nm, accordingly.
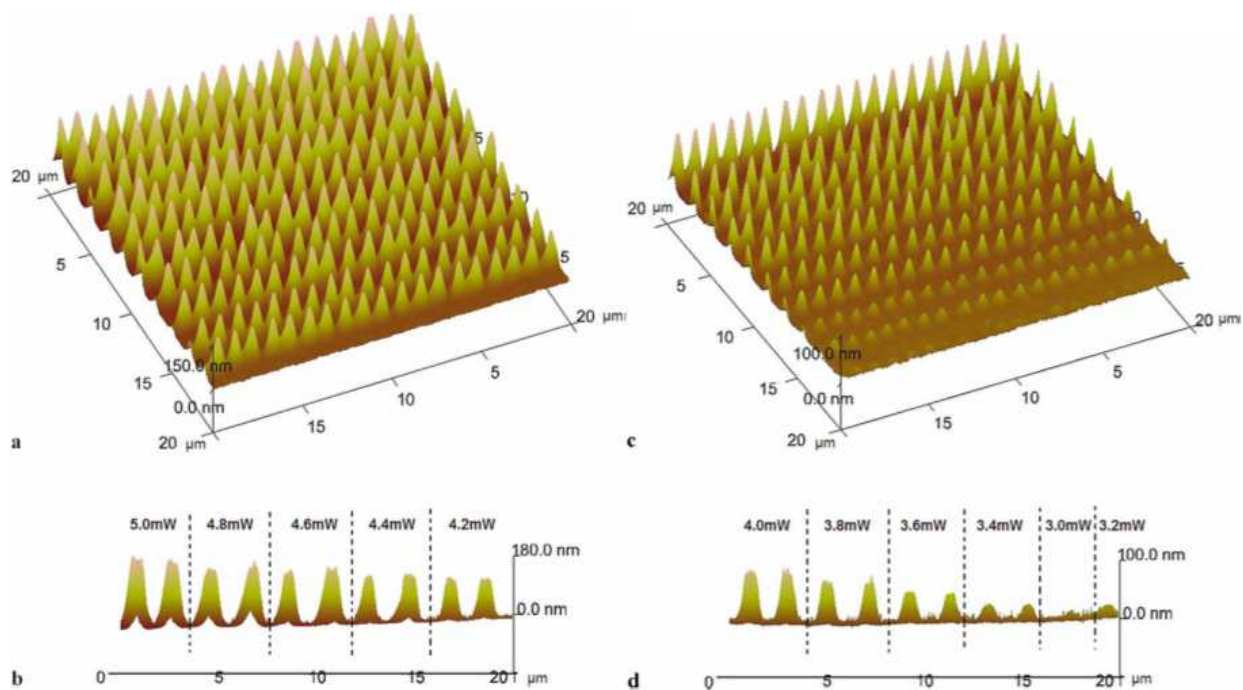

Fig. 11. Pattern structures written on multilayered ZnS–SiO2/AgOx/ZnS–SiO2 films by green laser (λ = 488 nm) in different laser processing parameters. (a) The AFM 3D photos of pattern structures written by higher laser power. (b) The lateral photos of the pattern structures in (a). (c) The AFM 3D photos of pattern structures written by lower laser power. (d) The lateral photos of the pattern structures in (c).

In order to test the stability of the pattern structure, we heated the sample shown in Fig. 11(a) in the furnace and kept the temperature at 100°C for 1 h. The result measured by AFM is shown in Fig. 14(a), and Fig. 14(b) is the lateral photo of Fig. 14(a). As shown in the photos, the taper shape does not change even if the temperature is kept at 100°C , and the regular and uniform pattern structures are almost the same as Fig. 11(a). Besides of that, one can see both the diameters and the heights gradually decreased with the laser power decreasing. The range of the height is from 100 nm to 180 nm, and the diameter is from 500 nm to 900 nm, correspondingly, which is very close to the values in Fig. 11(a), so we can conclude that the pattern structure was stable even if the temperature is higher than room temperature. We think that there are two main reasons. One is that AgOx material in this micro-zone is all decomposed under the laser irradiation with only Ag particles left. The other is that the layer structure is not a completely enclosed system, inter-diffusion between the gas in the bump and the air outside causes the pressure inside and outside the bump to reach a balance, and also the temperature is gradually increased. That is to say, in this gradual heating process, the gas in and out of the structure has enough time to inter-diffuse to reach a balance, so the structures can keep the same as before. The further explanation will be studied in our next work.
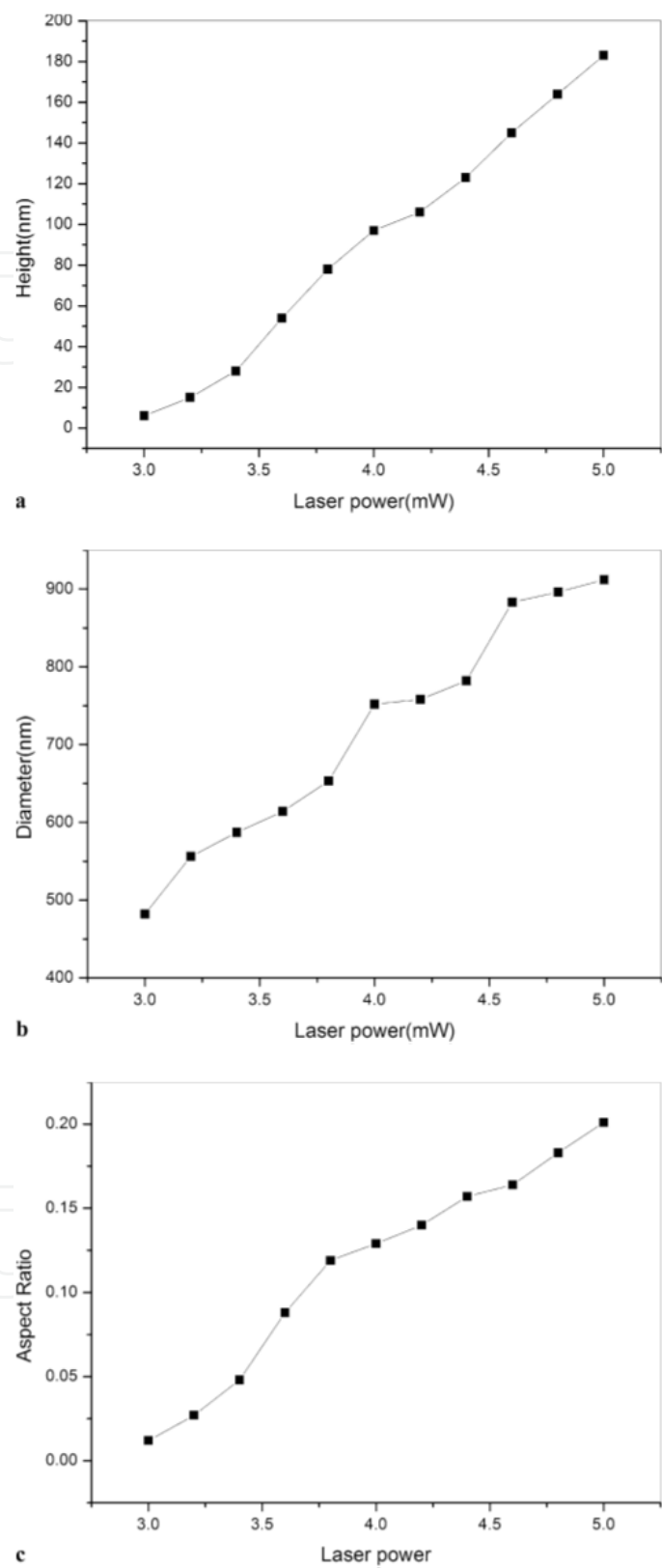
Fig. 12. Dependence of the pattern structures parameters on the laser power. (a) Dependence of height on laser power. (b) Dependence of diameter on laser power. (c) Dependence of aspect ratio on laser power
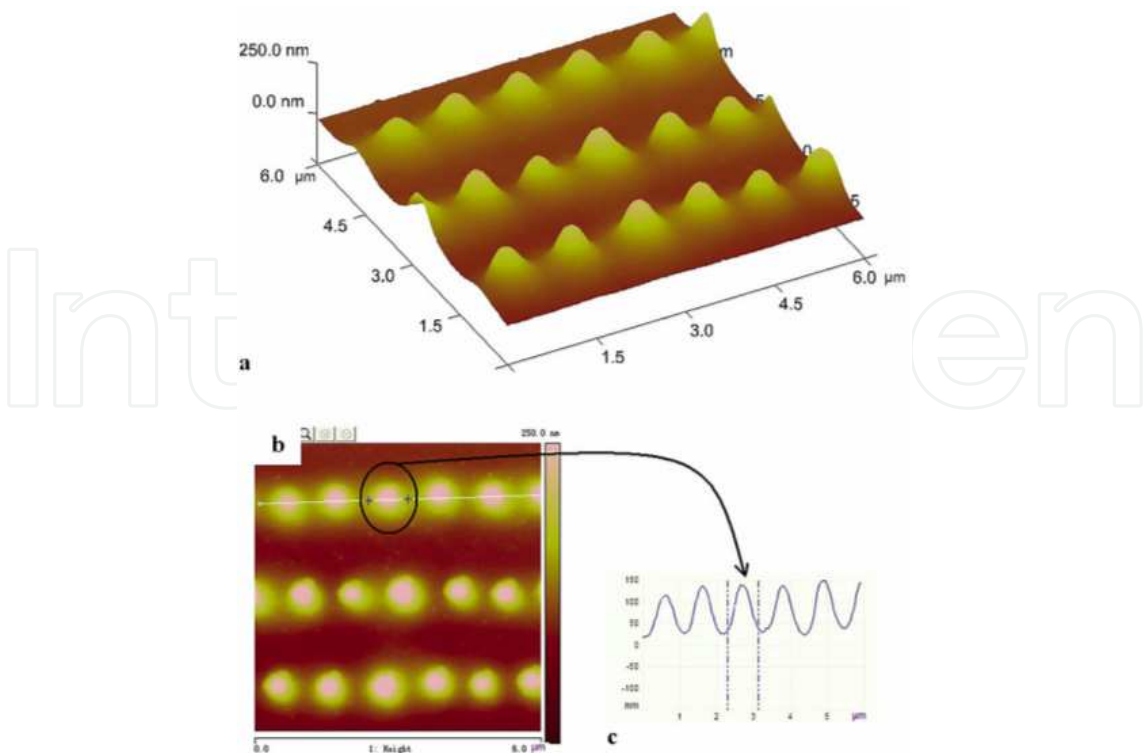
Fig. 13. Amplification photos of pattern structures chosen from Fig. 3(a). (a) The AFM 3D photos of pattern structure. (b) The chosen area of AFM analysis (marked by the line). c) AFM analysis of the pattern structure in (b).
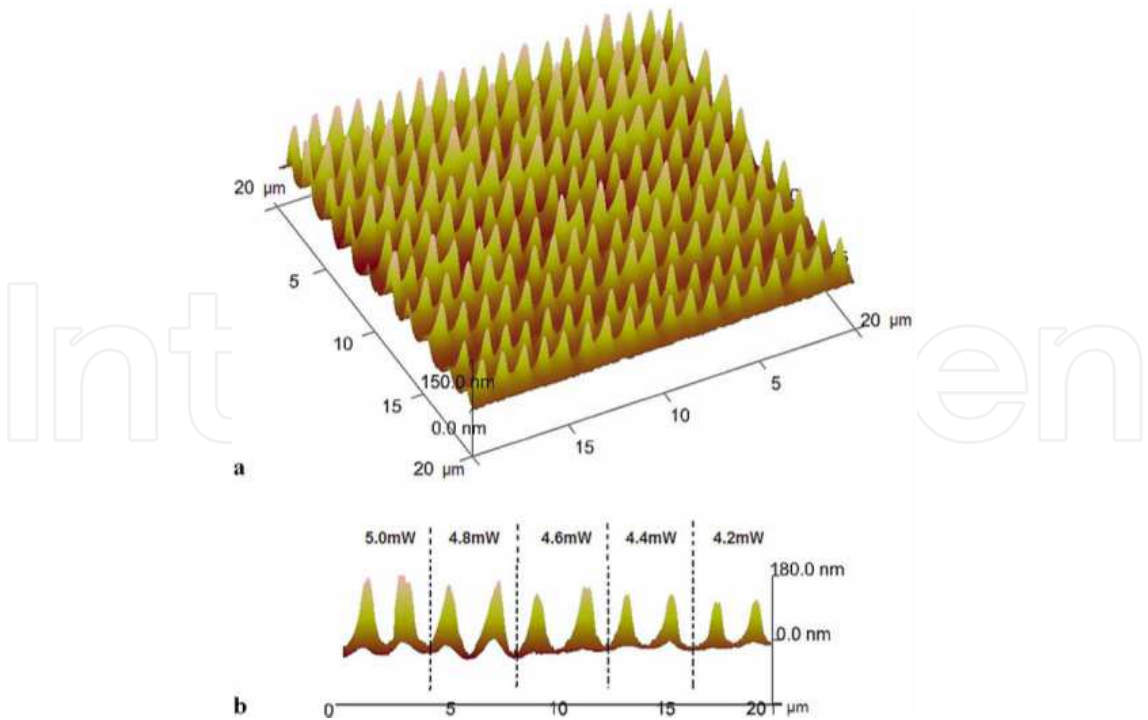

Fig. 14. AFM 3D photos of pattern structures in Fig. 3(a) kept the temperature at 100°C for 1 h. (a) The AFM 3D photos of pattern structures. (b) The lateral photos of the pattern structures in (a).

4. Conclusion

A theoretical model has been established for the bump formation in the optical writing process. Based on the developed formalism, geometric characters of the formed bumps can be analytically and quantitatively evaluated from various parameters involved in the formation. Simulations based on the analytic solution have been carried out taking $Ag_8In_{14}Sb_{55}Te_{23}$ as an example. The results have been verified with experimental observations of the bumps. It has been verified that the results from the simulations are consistent with the experimental observations. Micro/nanometric pattern structures have been fabricated on "ZnS–SiO2/AgOx/ZnS–SiO2" multilayer thin film sample by laser direct writing method. The pattern structures with different shapes and sizes could be directly written by very low laser power without developing and etching procedures, which could largely decrease the time-consuming and cost.

5. Acknowledgment

6. References

Wuttig R. and Steimer C. (2007). Phase change materials: From material science to novel storage devices. *Applied Physics A*, Vol.87, No.3, (June 2007), pp. 411-417, ISSN 1432-0630

Kolobov A. V., Fons P., Frenkel A. I., Ankudinov A. L., Tominaga J., and Uruga T. (2004). Understanding the phase-change mechanism of rewritable optical media. *Nature Materials*, Vol.3, No.10, (October 2004), pp. 703-708, ISSN 1476-1122

Welnic W., Parnungkas A., Detemple R., Steimer C., Blugel S., and Wuttig M., (2006). Unravelling the interplay of local structure and physical properties in phase-change materials. *Nature Materials*, Vol.5, No.1, (January 2006), pp. 56-62, ISSN 1476-1122

Kalb J., Spaepen F., and Wuttig M. (2004). Atomic force microscopy measurements of crystal nucleation and growth rates in thin films of amorphous Te alloys. *Applied Physics Letters*, Vol.84, No.25, (June 2004), pp. 56-62, ISSN 0003-6951

Wei J., Jiao X., Gan F. and Xiao M. (2008). Laser pulse induced bumps in chalcogenide phase change films. *Journal of Applied Physics*, Vol.103, No.12, (June 2008), pp. 124516-5, ISSN 0021-8979

Dun A. Wei J. And Gan F. (2010). Pattern structures fabricated on ZnS–SiO2/AgOx/ZnS–SiO2 thin film structure by laser direct writing technology. *Applied Physics A*, Vol.100, No.2, (August 2010), pp. 401-407, ISSN 1432-0630

Shiu T., Grigoropoulos C. P., Cahill D. G., and Greif R. (1999). Mechanism of bump formation on glass substrates during laser texturing. *Journal of Applied Physics*, Vol.86, No.3, (August 1999), pp. 1311-6, ISSN 0021-8979

Tominaga J., Haratani S., Uchiyama K., and Takayama S. (1992). New Recordable Compact Disc with Inorganic Material, AgOx. *Japaness Journal of Applied Physics*, Vol.31, No.9A, (September 1992), pp. 2757-2759, ISSN 0021-4922

Liu W.C., Wen C.Y., Chen K.H., Lin W.C., and Tsai D.P. (2001). Near-field images of the AgOx-type super-resolution near-field structure. *Applied Physics Letters*, Vol.78, No.6, (February 2001), pp. 685-687, ISSN 0003-6951
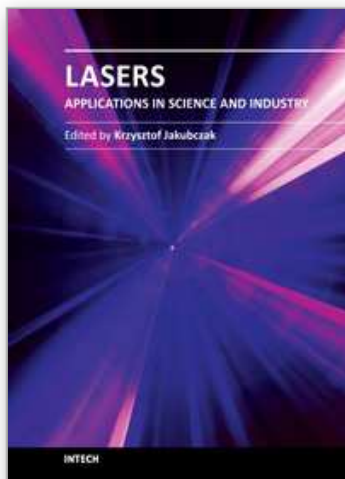
Lasers - Applications in Science and Industry

Edited by Dr Krzysztof Jakubczak

The book starts with basic overview of physical phenomena on laser-matter interaction. Then it is followed by presentation of a number of laser applications in the nano-particles and thin films production, materials examination for industry, biological applications (in-vitro fertilization,tissue ablation) and long-range detection issues by LIDARs.

How to reference

In order to correctly reference this scholarly work, feel free to copy and paste the following:

Jingsong Wei and Mufei Xiao (2011). Laser Pulse Patterning on Phase Change Thin Films, Lasers - Applications in Science and Industry, Dr Krzysztof Jakubczak (Ed.), ISBN: 978-953-307-755-0, InTech, Available from: http://www.intechopen.com/books/lasers-applications-in-science-and-industry/laser-pulse-patterning-on-phase-change-thin-films

INTECH
open science | open minds